LA-9516-MS

Los Alamos National Laboratory is operated by the University of California for the United States Department of Energy under contract W-7405-ENG-36.

Dimensionless Equation of State for Condensed Media—Numerical Results for Shock Heating and for Flow Deflection by an Oblique Stationary Shock

Los Alamos National Laboratory
Los Alamos, New Mexico 87545

This work was supported by the US Air Force.

LA-9516-MS

UC-34
Issued: September 1982

Dimensionless Equation of State for Condensed Media—Numerical Results for Shock Heating and for Flow Deflection by an Oblique Stationary Shock

J. M. Walsh

Los Alamos National Laboratory
Los Alamos, New Mexico 87545

DIMENSIONLESS EQUATION OF STATE FOR CONDENSED MEDIA-- NUMERICAL RESULTS FOR SHOCK HEATING AND FOR FLOW DEFLECTION BY AN OBLIQUE STATIONARY SHOCK

by

J. M. Walsh

ABSTRACT

A dimensionless equation-of-state formulation causes the solutions to a few standard problems in shock hydrodynamics to be somewhat more general than usual. Calculated results are given for shock heating and for the important problem of flow deflection by an oblique shock. The results will be useful on occasion because they can be applied without having to resort to extensive calculations for each new application.

I. INTRODUCTION

It is well known that analytical and even numerical solutions in fluid dynamics can be generalized if one can utilize a dimensionless equation of state that leads to material scaling laws.

The present dimensionless formulation (in addition to making a couple of customary approximations) incorporates the experimental shock-wave velocity versus shock-particle velocity slope, S, in such a way that the various Hugoniot curves coincide. Further, for part of the discussion, the weak dependence of fluid dynamics upon thermal expansion is utilized by assuming that the pertinent thermodynamic parameter (Grüneisen ratio divided by S) is the same for all materials. Under this assumption, all equation-of-state surfaces coincide.

Then some hydrodynamic results are more general. For example, a universal curve is obtained for dimensionless shock heating (i.e., heat deposited by combined shock and rarefaction) as a function of dimensionless shock pressure. Other results are generalized but not universal. The important problem of flow deflection by a standing shock front has a (numerical) solution that depends

upon a single material property, namely S. A general discussion is still possible, but S has to be varied as a parameter in the calculations.

The reported results for shock heating and for flow deflection may be useful because they can be scaled to any suitable material without having to exercise a high speed computer for each new application.

II. GOVERNING EQUATIONS

For the shock front, one has the usual jump conditions

$$P - P_o = \rho_o U_s U_p \quad , \tag{1}$$

$$(1 - V/V_o) = U_p/U_s \quad , \tag{2}$$

and

$$E - E_o = (P + P_o)(V_o - V)/2 \quad , \tag{3}$$

where E_o and P_o can be taken to be zero.

The continuous flow between shocks can be taken to be isentropic so that

$$dE = -PdV \quad . \tag{4}$$

With this assumption one obtains the usual equations that govern the isentropic continuous flow of a compressible fluid

$$\frac{\partial \rho}{\partial t} + \frac{\partial}{\partial x_i} (\rho U_i) = 0 \tag{5}$$

and

$$\rho \frac{\partial U_i}{\partial t} + U_i\left(\frac{\partial U_i}{\partial x_i}\right) = -\partial P/\partial x_i = -C^2 \frac{\partial \rho}{\partial x_i} \quad , \tag{6}$$

where

$$C^2 = (\partial P/\partial \rho)_s \quad .$$

Recall further that a continuous plane wave that propagates into a constant state (U_1, ρ_1, P_1) is a simple wave within which the particle velocity is given by the Riemann integral

$$U - U_1 = -\int_{\rho_1}^{\rho} \frac{C d\rho}{\rho} = -\int_{P_1}^{P} \sqrt{-dP dV} \quad . \tag{7}$$

Here, the second form of the integral is obtained by using $C^2 = (\partial P/\partial \rho)_s$ and $\rho = 1/V$. In either form the integration is to be performed along the isentrope.

III. MATERIAL PROPERTIES

Four properties are needed to characterize a material. These are the initial density ρ_0, the constants C_0 and S in the empirical relationship

$$U_s = C_0 + SU_p \tag{8}$$

for shock-wave velocity as a function or shock-particle velocity, and the thermodynamic quantity

$$(\partial P/\partial E)_V \equiv \rho\gamma \quad . \tag{9}$$

Here, γ is Grüneisen ratio.

It has long been recognized* that the simple linear relation, Eq. (8), is a remarkably good analytical fit to the shock-wave data for many materials. Values of C_o and S for a few materials of interest, extracted from Marsh's compendium, are listed in Table I.

Further, the quantity $(\partial P/\partial E)_V$ is used only to estimate the generally small offsets between the experimental Hugoniot curve [the consequence of Eq. (8)] and neighboring isentropes. It is accurate enough for present purposes to assume that $(\partial P/\partial E)_V$ is constant; that is,

$$\rho\gamma = \rho_o\gamma_o \quad . \tag{10}$$

IV. DIMENSIONLESS VARIABLES

Define:

$$p = PS/\rho_o C_o^2 = \text{pressure} \quad , \tag{11}$$

$$\eta = S(1 - V/V_o) = \text{compression} \quad , \tag{12}$$

$$e = S^2 E/C_o^2 = \text{specific internal energy} \quad , \tag{13}$$

and

$$u = SU/C_o = \text{mass velocity} \quad . \tag{14}$$

*R. G. McQueen and S. P. Marsh, "Equation of State of Nineteen Metallic Elements from Shock Wave Measurements," Journal of Applied Physics 31, p. 1253 (1960). See also a recent compendium of shock-wave data "LASL Shock Hugoniot Data," S. P. Marsh, University of California Press (1980).

The governing equations that were listed as Section II can now be rewritten in terms of these dimensionless variables. Equation (8) becomes

$$\frac{U_s}{C_o} = (1 + u) \quad . \tag{15}$$

Equations (1), (2), and (3) become (dropping P_o and E_o)

$$p = (1 + u)u \quad , \tag{16}$$

$$\eta = u/(1 + u) \quad , \tag{17}$$

and

$$e = p\eta/2 \quad . \tag{18}$$

Solving Eqs. (16) and (17) gives the Hugoniot curve

$$p = \frac{\eta}{(1 - \eta)^2} \quad , \tag{19}$$

and the expression for u

$$u = (\sqrt{1 + 4p} - 1)/2 \quad . \tag{20}$$

Equation (4) becomes

$$de = pd\eta \quad . \tag{21}$$

Equation (7) becomes

$$u = u_1 - \int_{p_1}^{p} \sqrt{dp\,d\eta} \quad , \tag{22}$$

and Eqs. (9) and (10) can be combined to give

$$\left(\frac{\partial p}{\partial e}\right)_{\eta} = \gamma_0/S \equiv \beta \quad . \tag{23}$$

The new variables cause some of the above equations [Eqs. (16)-(22)] to be universal in the sense that material properties do not appear explicitly. Others are less general. Equation (23), for example, involves us with the material property $\beta = \gamma_0/S$, and the expression for shock wave velocity, Eq. (15), lacks a factor S that is needed to make it correspond to the mass velocity, Eq. (14).

Solutions to flow problems obtained from the universal equations only are applicable to any material by a simple change in scale factors. Solutions from property-dependent equations, on the other hand, contain the material properties as parameters. If the latter results are numerical, in particular, the flow problem must be calculated for a range of values of the pertinent material parameters.

V. DIMENSIONLESS EQUATION OF STATE, ISENTROPES, RIEMANN INTEGRALS, AND SHOCK HEATING

Integrating Eq. (23) and using Eqs. (18) and (19) gives the equation of state

$$p = p_h(\eta) + \beta\left(e - \frac{\eta p_h(\eta)}{2}\right) \quad , \tag{24}$$

where

$$p_h(\eta) = \frac{\eta}{(1 - \eta)^2} \quad .$$

The differential equation for the family of isentropes is obtained by substituting Eq. (21) into the derivative of Eq. (24),

$$2dp = 2dp_h + \beta(2pd\eta - p_h d\eta - \eta dp_h) \quad . \tag{25}$$

Numerical solutions of Eq. (25), to give the isentropes that intersect the Hugoniot at p = 0.5, 1.0, 1.5, and 2.0, are plotted as Fig. 1. To calculate the isentropes a value $\beta = 1.3$ was used, corresponding to a typical value of this material property (see Table I).

Riemann integrals, Eq. (22), were also calculated for the isentropes and are plotted in Fig. 2 (curves of negative slope). Here, p_1, u_1 in Eq. (22) was taken as the point on the Hugoniot, which is plotted as the curve of positive slope. Thus, the curves in Fig. 2 correspond to right-going shocks reflected from free surfaces as left-going rarefactions. The associated specific internal energies are calculated from Eqs. (18) and (21).

Of frequent interest is the heating caused by combined shock and rarefaction to zero pressure. These results are seen as Fig. 3 where the dimensionless residual specific internal energy ($q = S^2E/C_0^2$) is plotted versus dimensionless shock pressure.

The three curves given for q in Fig. 3 are for values $\beta = 1.0$, 1.3, and 1.6. Most materials lie within this β range, as do 16 of the 20 materials listed in Table I. Riemann integrals were also calculated with the varied values of β but were everywhere affected less than 2% (up to p = 5).

The observed insensitivity to β of the computed results suggests (for the analysis of shock-hydrodynamic flows involving shocks of a couple megabars or less, or when accuracy is more important than generality) that an average value of β, such as $\beta = 1.3$, can be used for all materials. For example, a 1-Mbar shock in 2024 aluminum ($\rho_0 = 2.785$ g/cm^3, $C_0 = 5.328 \times 10^5$ cm/s, S = 1.338) has

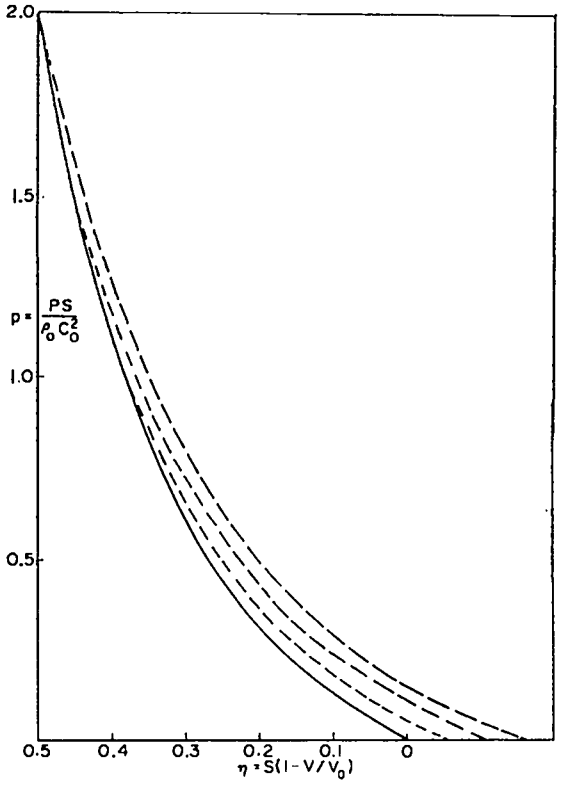

Fig. 1. Hugoniot and isentropes. Isentropes calculated assuming $\beta = 1.3$.

TABLE 1

MATERIAL PROPERTIES

	ρ_0(g/cm^3)	C_0(km/s)	S	γ_0	$\beta = \gamma_0/S$	$\rho_0 C_0^2$(Mbar)
Antimony	6.7	1.983	1.652	0.60	0.363	0.263
Beryllium	1.851	7.998	1.124	1.16	1.03	1.184
Chromium	7.117	5.173	1.473	1.19	0.81	1.904
Copper	8.93	3.940	1.489	1.99	1.34	1.386
Gold	19.24	3.056	1.572	2.97	1.89	1.797
Lead	11.35	2.051	1.460	2.77	1.90	0.477
Magnesium	1.74	4.492	1.263	1.42	1.12	0.351
Molybdenum	10.21	5.124	1.233	1.52	1.23	2.681
Nickel	8.874	4.602	1.437	1.93	1.34	1.879
Niobium	8.586	4.438	1.207	1.47	1.22	1.691
Palladium	11.991	3.948	1.588	2.26	1.42	1.869
Platinum	21.42	3.598	1.544	2.40	1.55	2.773
Silver	10.49	3.229	1.595	2.38	1.49	1.094
Tantalum	16.654	3.414	1.201	1.60	1.33	1.941
Thorium	11.680	2.133	1.263	1.26	1.00	0.531
Tungsten	19.224	4.029	1.237	1.54	1.25	3.120
Uranium	18.950	2.487	1.56	2.20	1.41	1.172
Brass	8.450	3.726	1.434	2.04	1.42	1.173
2024 Aluminum	2.785	5.328	1.338	2.00	1.50	0.790
304 Stainless Steel	7.896	4.569	1.490	2.17	1.46	1.648

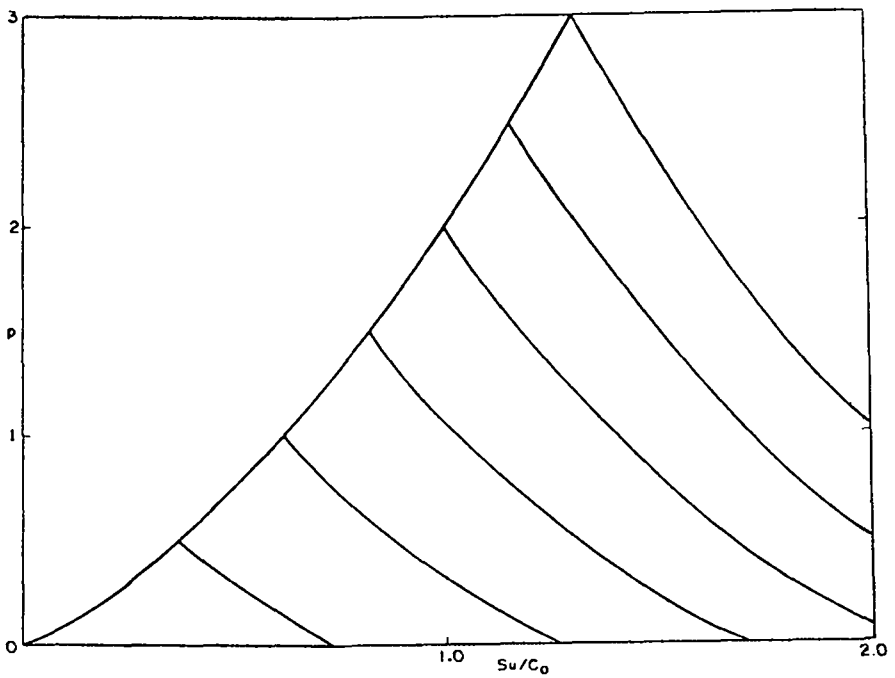

Fig. 2. Dimensionless p versus u curves from the Hugoniot and isentropes seen in Fig. 1.

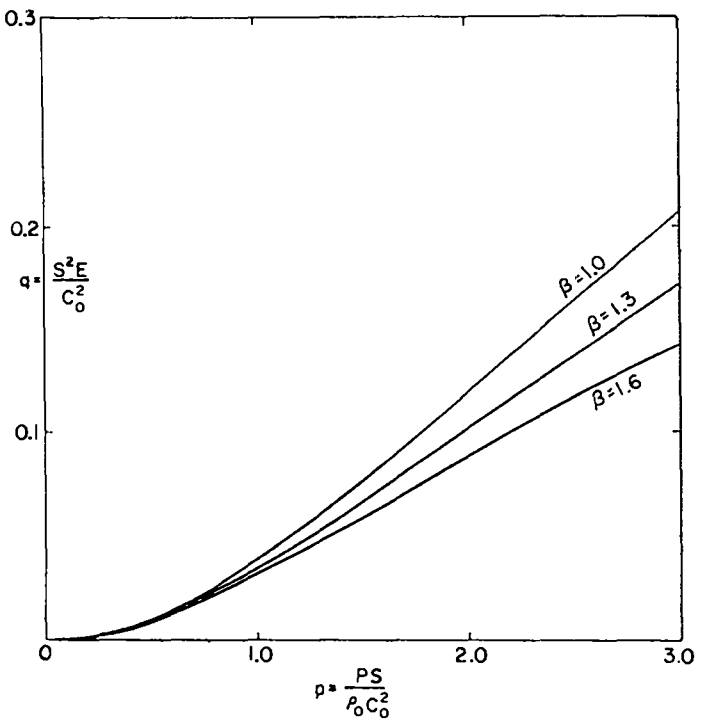

Fig. 3. Shock heating by combined shock and rarefaction to zero pressure as a function of shock pressure.

a dimensionless shock pressure

$$p = \frac{PS}{\rho_o C_o^2} = 1.692 \quad .$$

The associated dimensionless shock heating and free surface velocity (see Figs. 2 and 3) are q = 0.81 and u = 1.843. The last two values in dimensional form are

$$Q = \frac{qC_o^2}{S^2} = 12.87 \times 10^{10} \text{ ergs/g}$$

and

$$U_{fs} = \frac{C_o U}{S} = 7.331 \times 10^5 \text{ cm/s} \quad .$$

Had the Table I value of $\beta = 1.5$ for aluminum been used for accuracy, Q would have been 8.8% lower, and U_{fs} would have been only about 0.4% higher.

VI. THE SHOCK DEFLECTION PROBLEM

The shock deflection problem arises frequently as part of a more complex problem. Examples are the oblique interaction of a shock with a material interface, or the collision of two material surfaces with a supersonic phase velocity.

Let U_o (supersonic, horizontally directed) be entry flow velocity to the stationary shock, and let U_h and U_v be the horizontal and vertical components of velocity. Figure 4 illustrates this situation and defines variables used in the

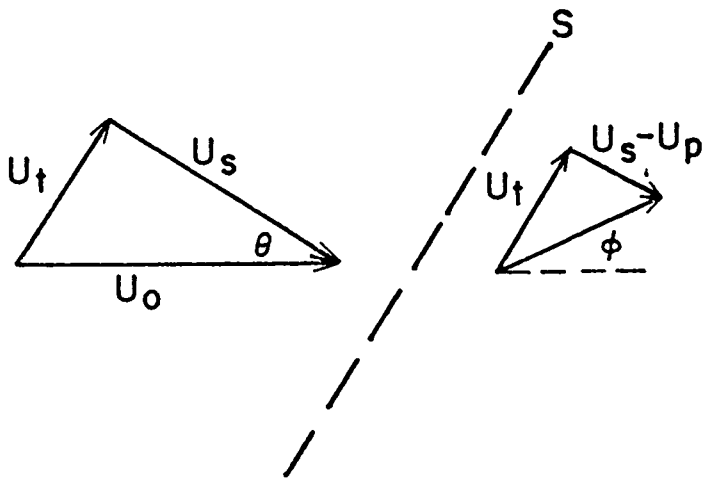

Fig. 4. Flow deflection through ϕ as caused by a stationary shock. Shock orientation relative to U_o is given by θ.

present problem, and Fig. 5 is the associated shock polar diagram. In Fig. 5, U_o is resolved into its two components normal and tangent to the shock front,

$$U_s = U_o \cos \theta \tag{26}$$

and

$$U_t = U_o \sin \theta \tag{27}$$

by any point on the (dashed) semicircle. The inner (solid) curve is the shock polar and is the locus of points attainable by shocks of various inclinations θ and shock-particle velocities U_p. Now, Eqs. (8) and (26) imply that the equation for shock polar is

$$U_p = \frac{U_o \cos \theta - C_o}{S} \quad . \tag{28}$$

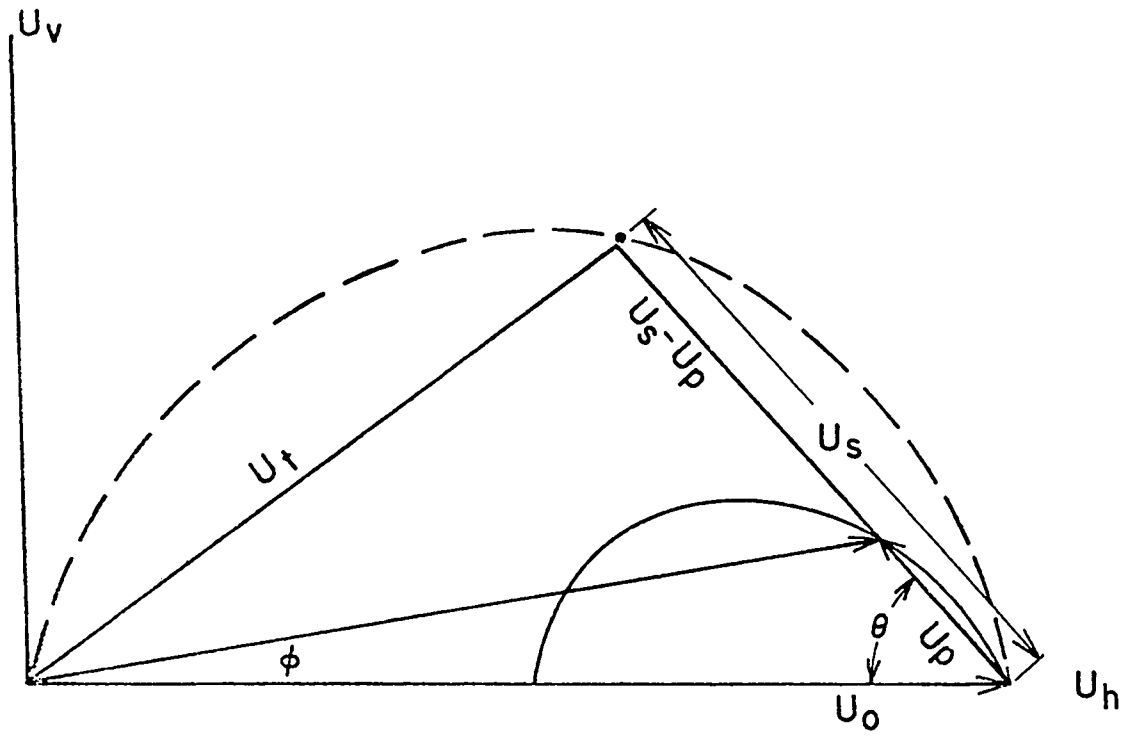

Fig. 5. Shock polar diagram for given entry-flow velocity U_o.

Further, see Fig. 5, the flow deflection angle ϕ is given by

$$\phi = (90° - \theta) - \tan^{-1}\left(\frac{U_s - U_p}{U_t}\right) . \tag{29}$$

For the discussion below of shock polars, it is convenient to introduce velocities in units of U_o/S. Thus, the entry-flow velocity U_o becomes just S. Shock-particle velocity becomes

$$\left(\frac{SU_p}{U_o}\right) ,$$

and the equation for shock-particle velocity, Eq. (28), becomes

$$\left(\frac{SU_p}{U_o}\right) = \cos\theta - 1/M \quad , \tag{28'}$$

where $M = U_o/C_o$ is the Mach number in the entry flow. The expression for shock velocity, from Eqs. (8) and (28'), is

$$\left(\frac{SU_s}{U_o}\right) = S\cos\theta \quad ,$$

and the expression $U_t = \sqrt{U_o^2 - U_s^2}$ becomes

$$\left(\frac{SU_t}{U_o}\right) = S\sin\theta \quad .$$

Using these last three equations, Eq. (29) for flow deflection becomes

$$\phi = (90^\circ - \theta) - \tan^{-1}\left(\frac{S\cos\theta - \cos\theta + 1/M}{S\sin\theta}\right) \quad . \tag{29'}$$

From Eqs. (16), (17), (18), and (28'), and noting that u in the earlier equations is just

$$u = M\left(\frac{SU_p}{U_o}\right) \quad ,$$

we have

$$p = M^2 \cos^2 \theta - M \cos \theta \quad , \tag{30}$$

$$\eta = 1 - \left(\frac{1}{M \cos \theta}\right) \quad , \tag{31}$$

and

$$e = (M \cos \theta - 1)^2/2 \quad . \tag{32}$$

Thus, the shock strength (p, n, or e) is a maximum [M(M-1), (M-1)/M, or $(M-1)^2/2$] at $\theta = 0$ and decreases with increasing θ to zero at $\theta = \cos^{-1}(1/M)$ at which minimum value of θ the shock is just a sound wave.

The family of shock polars, for various values of the entry-flow Mach number M, is plotted as Fig. 6. The polar for $M = \infty$ is the semicircle

$$\left(\frac{SU_p}{U_o}\right) = \cos \theta \quad ,$$

see Eq. (28'), with diameter extending from (S-1,0.) to (S,0.). A polar for any given $M = M_1$ is obtained by offsetting (toward S,0.) each point on the semicircle by an amount $1/M_1$.

The maximum possible flow deflection ϕ, for given M and S, is the point at which the polar is tangent to the straight line from the origin. Three loci of such critical points, for selected (S = 1.2, S = 1.4, and S = 1.6) values of S, are plotted on Fig. 6 as dashed lines. [These critical points were obtained numerically by maximizing the expression for ϕ, Eq. (29').]

Because the shock is oblique the exit flow may be subsonic, sonic, or supersonic. At $\theta = 0$, the shock is normal so the exit flow is clearly subsonic.

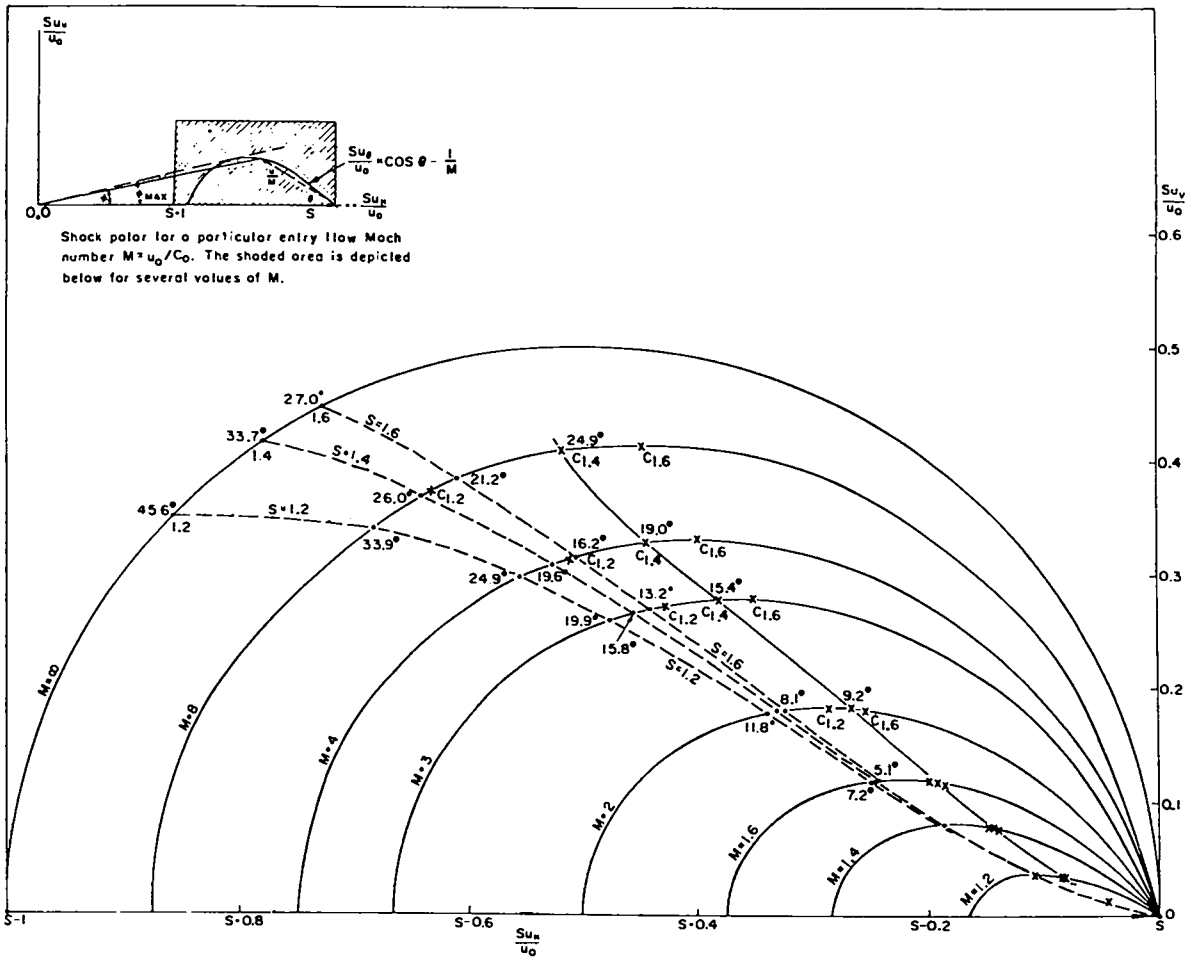

Fig. 6. Eight shock polars for varied values of the entry-flow Mach number. All velocities are in units U_o/S. The three dashed curves (for S = 1.2, 1.4, and 1.6) are loci of the maximum-deflection critical angle ϕ_{max}. The points plotted as x's and labelled $C_{1.2}$, $C_{1.4}$, and $C_{1.6}$ (for S = 1.2, 1.4, and 1.6) are the points of sonic exit flow. Values of ϕ are written beside critical points and sonic points.

At the other end [θ - arc cos (1/M)] of the polar, the flow remains supersonic across the (zero strength) shock. In between there is a point of exactly sonic flow. Here, then (see Fig. 5)

$$C^2 = U_t^2 + \left(U_s - U_p\right)^2$$

or, equivalently

$$a^2 = M^2\left[(S \sin\theta)^2 + \left(S\cos\theta - \left(\cos\theta - \frac{1}{M}\right)\right)^2\right] \quad , \tag{33}$$

where the dimensionless sound speed a is given by

$$a^2 = \frac{S^2 C^2}{C_o^2} \quad . \tag{34}$$

This last expression, using $C^2 = (\partial p/\partial \rho)_J$, $\rho = 1/V$, and Eqs. (12), (21), and (25), becomes

$$a^2 = \left[\frac{\eta + 1 - \beta\eta^2}{(1-\eta)^3}\right](S - \eta)^2 \quad . \tag{35}$$

Equating the right sides of Eqs. (33) and (35), and using Eq. (31) to eliminate η, gives one an equation for θ at the sonic point as a function of M and the <u>two</u> material properties β and S. Once this θ is known, the other quantities associated with the sonic point are easily determined from Eqs. (28'), (29'), and (30)-(32). Sonic points have been calculated using $\beta = 1.5$ and three values (S = 1.2, S = 1.4, and S = 1.6) of the parameter S. These sonic points are plotted as x's on the polar diagrams in Fig. 6 and are labelled $C_{1.2}$, $C_{1.4}$, and $C_{1.6}$, respectively. It is seen there that the sonic points lie to the right of the correspondingly critical angle in each case. Thus, for given flow deflection ϕ, the strong shock solution is characterized by subsonic exit flow in each case, while the weak shock solution may have either subsonic or supersonic exit flow.

VII. PROBLEM EXAMPLES INVOLVING SHOCK DEFLECTION

As a simple example, consider two copper plates (ρ_o = 8.93 g/cm^3, C_o = 3.94 x 10^5 cm/s, S = 1.489, see Table I) that impact at a 20° included angle, each with velocity 3 x 10^5 cm/s normal to its free surface. For this situation, the collapse phase velocity (units cgs) is 3 x 10^5/sin 10° = 1.727 x 10^6, the incoming stream velocity is 3 x 10^5/tan 10° = 1.701 x 10^6, and the entry-flow Mach number is

$$M = U_o/C_o = \frac{1.701 \times 10^6}{3.94 \times 10^5} = 4.32 \quad .$$

Equation (29') for these values becomes

$$10 = 90° - \theta - \tan^{-1}\left(\frac{1.489 \cos\theta - \cos\theta + 0.2315}{1.489 \sin\theta}\right)$$

with numerical solution $\theta = 59.5°$. Equations (30)-(32) then give p = 2.615, n = 0.544, and e = 0.711. The shock pressure

$$P = \frac{\rho_o C_o^2}{S} p = 2.43 \text{ Mbar}$$

is, as expected, somewhat higher than the 2.25 Mbar for head-on impact of the same plates. From Fig. 6 it is apparent (using $\theta = 59.5°$ and $M \doteq 4$, and comparing with the plotted sonic points) that the flow behind the present shocks is supersonic in the steady state of coordinate system.

The more general impact problem (asymmetric, and/or different materials) also involves the problem of flow deflection by shock and can be treated in much the same manner if an ideal slipstream is assumed to exist across the interface. Here the incoming stream velocities are, in general, different. Boundary conditions at the interface are pressure equality and common flow

direction. Thus, if ϕ_0 is the angle between the colliding surfaces, and $\phi_1(P)$ and $\phi_2(P)$ are deflections of the two streams, then

$$\phi_1(P) = \phi_0 - \phi_2(P) \quad .$$

The solution of this equation usually requires calculating $\phi_1(P)$ and $\phi_2(P)$ for several values of P by the method given in the preceding paragraph.

If ϕ_0 is increasing (consider a flat plate impacting a sphere), one obtains a shock pressure that increases as the impact progresses until a critical ϕ_0 is reached above which angle shock deflection of the impinging streams (totaling ϕ_0) is no longer possible. Thereafter, the impact process is more complicated with jetting occurring into the cavity between the colliding surfaces.

As another example, consider a shock of given (dimensionless) pressure p that arrives at a free surface or at an interface with a material of lower shock impedance. For interaction angle A (see Fig. 7) that is sufficiently small, one has the well-known situation in which the shock is completely unperturbed until it arrives at the surface (or interface) and the pressure is relieved by a Prandtl-Meyer expansion. Our interest here is in determining the critical angle A_c, separating this simple situation from the one that occurs at larger A, where the shock is attenuated by rarefaction from the free surface as it approaches the latter. Because p is fixed, Eq. (30) implies an M versus θ locus

$$p = M \cos \theta \, (M \cos \theta - 1)$$

that could be plotted in the shock polar plane (Fig. 6) where its position, relative to the sonic points, is then evident. Doing this for a shock strength p = 2 shows intersection with the sonic locus (for S = 1.4, β = 1.3) at $\theta = 36°$, M = 2.5. Thus, noting that $A = 90° - \theta$, the critical value A_c for p = 2 is seen to be 54°.

Figure 7 is a plot of A_c for a wide range of p. The solid line is for S = 1.4, and the dashed curves are for S = 1.2 and S = 1.6. In all cases, β was held constant at 1.5. Nearly all experiments with explosives are in the range p = 0.1 to p = 10 where $A_c = 60° \pm 10°$.

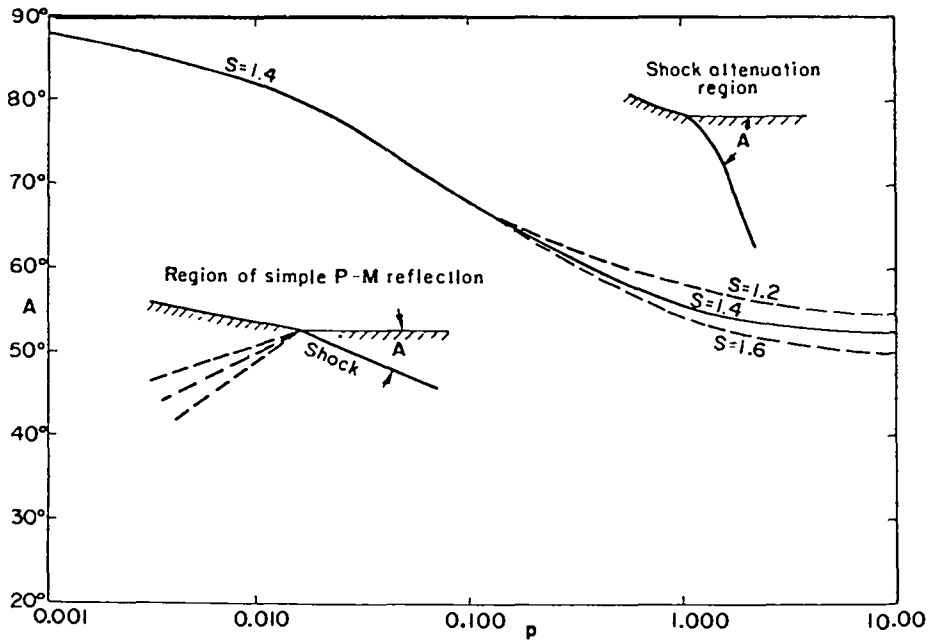

Fig. 7. Region of Prandtl-Meyer reflection at small A and shock attenuation region at large A.

Two other problems will be mentioned. The problem of shock reflection (either regular or Mach reflection) in condensed materials involves the consideration of doubly shocked states. Shock polars for the deflection of a previously shocked (arbitrary shock strength) state could obviously be constructed, but we have not considered that problem here.

Finally, the problem of a detonation wave that sweeps along a metal HE interface (variable angle of interaction) is of some interest. In this case the pertinent states ahead (the undetonated HE, the Chapman-Jouguet state of the HE, and the initial state of the metal) are few and fixed, and there is hope of an orderly and quantitative description of the phenomena involved. Considerable progress in this direction has, indeed, been made by Sternberg and Piacesi* and more recently by Melvin Thieme in unpublished calculations at Los Alamos. In our next discussion, we will consider this problem further and give calculated results for some HE-metal interactions of current interest.

*H. M. Sternberg and D. Piacesi, "Interaction of Oblique Detonation Waves with Iron," Physics of Fluids 9, No. 7, 1307-1351 (July 1966).

Printed in the United States of America
Available from
National Technical Information Service
US Department of Commerce
5285 Port Royal Road
Springfield, VA 22161

Microfiche (A01)

Page Range	NTIS Price Code	Page Range	NTIS Price Code	Page Range	NTIS Price Code	Page Range	NTIS Price Code
001-025	A02	151-175	A08	301-325	A14	451-475	A20
026-050	A03	176-200	A09	326-350	A15	476-500	A21
051-075	A04	201-225	A10	351-375	A16	501-525	A22
076-100	A05	226-250	A11	376-400	A17	526-550	A23
101-125	A06	251-275	A12	401-425	A18	551-575	A24
126-150	A07	276-300	A13	426-450	A19	576-600	A25
						601-up*	A99

*Contact NTIS for a price quote.

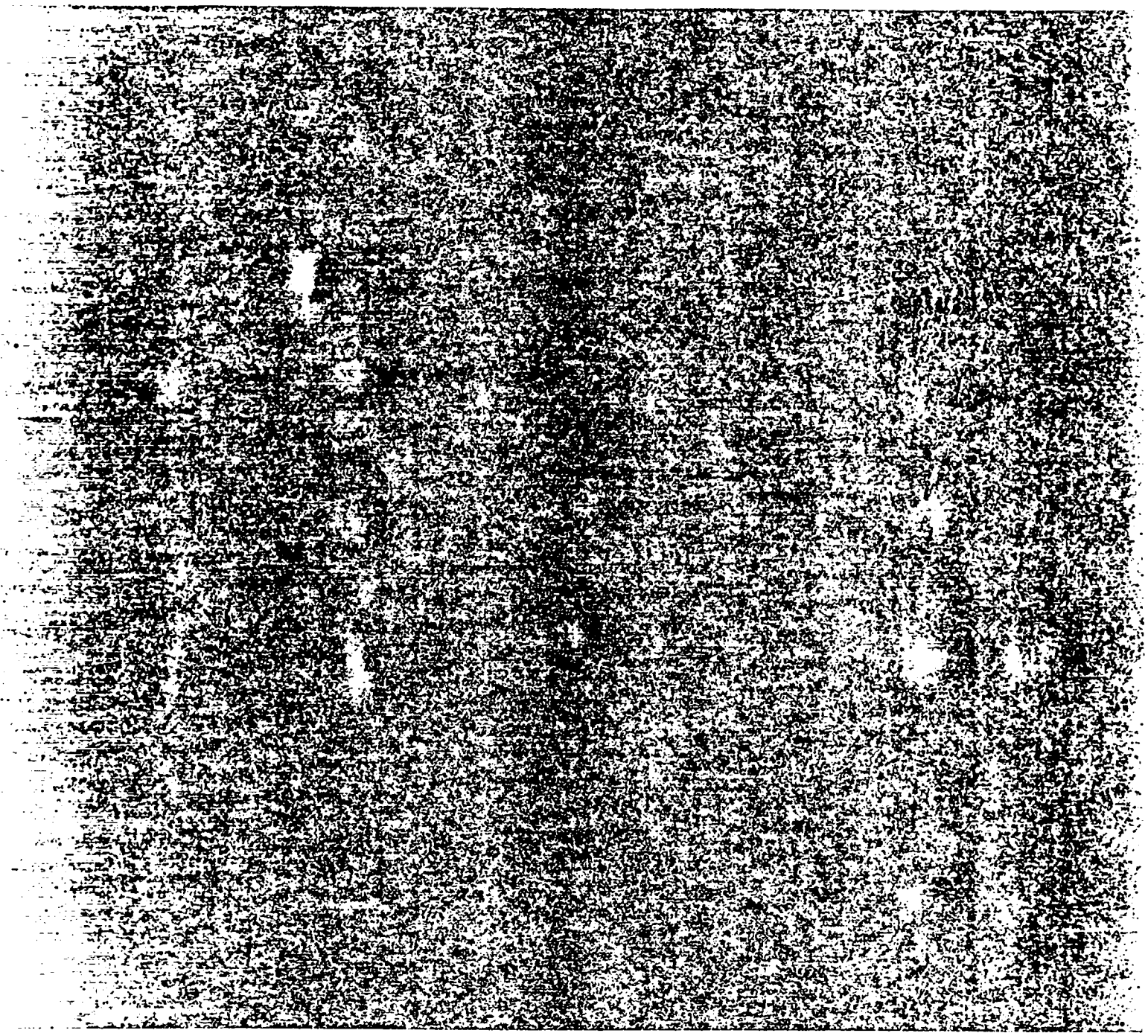

Los Alamos